



Cite this: *Chem. Commun.*, 2019, 55, 8118

Received 12th March 2019,
Accepted 25th April 2019

DOI: 10.1039/c9cc02006c

rsc.li/chemcomm

Low-temperature synthesized $\text{Li}_4\text{Mn}_5\text{O}_{12}$ -like cathode with hybrid cation- and anion-redox capacities†

Yang Liu,^{ab} Guang Liu,^{ab} Hui Xu,^{ab} Yuheng Zheng,^{ab} Yunhui Huang,^{ab}
Sa Li^{*ab} and Ju Li^{id *c}

The Li-rich spinel $\text{Li}_4\text{Mn}_5\text{O}_{12}$ ($\text{Li}(\text{Mn}_{5/3}\text{Li}_{1/3})\text{O}_4$) historically only shows a reversible cation-redox reaction, with a theoretical capacity of $135.5 \text{ mA h g}^{-1}$. However, we found that a simple 400°C solid-state synthesis method gives a $\text{Li}_4\text{Mn}_5\text{O}_{12}$ -like nanoparticulate cathode that yields significant reversible hybrid cation- and anion-redox capacities. A high specific capacity of 212 mA h g^{-1} was achieved. The reversible anion-redox contribution is attributed to the tiny particle size ($<10 \text{ nm}$), which facilitates electron tunneling, and a possible random solid-solution in the $\text{Li}(\text{Mn}_{5/3}\text{Li}_{1/3})\text{O}_4$ lattice due to the low synthesis temperature.

Although the spinel $\text{Li}_4\text{Mn}_5\text{O}_{12}$ is cost-effective¹ and environment-friendly without the expensive and toxic Co or Ni, it has significant challenges to meet the demands of rechargeable batteries. Among them, the relatively low specific capacity has been a bottleneck ever since it was initially reported by M. M. Thackeray two decades ago.^{2,3} Starting with $\text{Li}_{4-m}^+\text{Mn}_5^{4+}\text{O}_{12}^{2-}$, because the Mn ions are already tetravalent, delithiation cannot occur⁴ without a concomitant change in the average oxygen valency as $\text{Li}_{4-m}^+\text{Mn}_5^{4+}\text{O}_{12}^{(2-a)-}$, where $a = m/12 \geq 0$ tracks the degree of oxygen anion-redox capacity at around $4 \text{ V vs. Li}^+/\text{Li}$.⁵⁻⁷ This was reportedly very difficult, or at least the capacity was highly irreversible. Upon the first net lithiation, a reversible capacity did emerge as $\text{Li}_4^+\text{Mn}_5^{4+}\text{O}_{12}^{2-} \leftrightarrow \text{Li}_{4+p}^+\text{Mn}_5^{(4-c)+}\text{O}_{12}^{2-}$, where $c = p/5 \geq 0$ tracks the degree of transition-metal cation-redox capacity. This part of the capacity at around $3 \text{ V vs. Li}^+/\text{Li}$ was practically seen to be reversible, and the spinel structure could be maintained as long as $p \leq 2.5$ ($c \leq 0.5$, $\text{Li}_{6.5}^+\text{Mn}_5^{3.5+}\text{O}_{12}^{2-}$), which gives a theoretical capacity of $135.5 \text{ mA h g}^{-1}$. If p was extended to 3 ($c = 0.6$, $\text{Li}_7^+\text{Mn}_5^{3.4+}\text{O}_{12}^{2-}$), the cation-redox theoretical capacity increased to $162.6 \text{ mA h g}^{-1}$, but the

cyclability was poor due to the Jahn-Teller distortion induced phase transformation. In addition to a low capacity and low voltage ($135.5 \text{ mA h g}^{-1}$ at 3 V), from the stand-point of making a practical Li-matched full cell using the $\text{Li}_4\text{Mn}_5\text{O}_{12}$ cathode against a graphite anode, the following challenges must be considered: (a) one must use pre-lithiated graphite or another lithium source to supply additional cyclable lithium for the first net lithiation $\text{Li}_4^+\text{Mn}_5^{4+}\text{O}_{12}^{2-} \rightarrow \text{Li}_{4+p}^+\text{Mn}_5^{(4-c)+}\text{O}_{12}^{2-}$, (b) there is going to be some Mn-ion dissolution in the liquid electrolyte, which aggressively attacks the graphite anode. For these reasons, $\text{Li}_4\text{Mn}_5\text{O}_{12}$ is not considered to be an attractive cathode material. Here, however, we will show that by a low-temperature synthesis at 400°C , we can make a nanostructured $\text{Li}_4\text{Mn}_5\text{O}_{12}$ -like material with both p,c -contribution (Mn cation redox capacity) and m,a -contribution (O anion redox capacity), giving a total reversible capacity of 212 mA h g^{-1} . Furthermore, by pairing with a pre-lithiated Sn metal anode in a standard carbonate electrolyte, the dissolved Mn-ion's attack on the anode seems to be less of a problem. This enables the stable cycling of a Li-matched full cell based on the $\text{Li}_4\text{Mn}_5\text{O}_{12}$ -like cathode for more than 100 cycles.

In previous reports, Takada *et al.* had synthesized a well-crystallized $\text{Li}_4\text{Mn}_5\text{O}_{12}$ with a rechargeable capacity of about 135 mA h g^{-1} at a voltage of $2.5\text{--}3.6 \text{ V}$ for only 10 cycles.⁸ Jiang *et al.* had reported that $\text{Li}_4\text{Mn}_5\text{O}_{12}$ prepared by spray-drying could deliver a discharge capacity of $157.8 \text{ mA h g}^{-1}$ at a voltage range of $2.4\text{--}3.7 \text{ V}$ and maintained 76% capacity retention after 80 cycles.⁹ Fu *et al.* found that $\text{Li}_4\text{Mn}_5\text{O}_{12}$ with hierarchical porous nano/micro structure had a capacity of 161 mA h g^{-1} at a voltage range of $2.0\text{--}3.5 \text{ V}$ and it maintained a capacity of about 89 mA h g^{-1} after 100 cycles at 0.5C .¹⁰ In most studies, the main capacity appears to originate from the p,c -contribution (Mn cation redox capacity) of $\text{Li}_4\text{Mn}_5\text{O}_{12} + 2.5\text{e}^- + 2.5\text{Li}^+ \rightarrow \text{Li}_{6.5}\text{Mn}_5\text{O}_{12}$ at a voltage of $\sim 3 \text{ V vs. Li}^+/\text{Li}$, and the four initial lithium ions were not active during the charge/discharge process. Moreover, doping strategies were also tried in order to enhance the energy density of $\text{Li}_4\text{Mn}_5\text{O}_{12}$, and the operating voltage was increased to 4.7 V , although there was no significant improvement in the capacity.¹¹

^a School of Materials Science and Engineering, Tongji University, Shanghai 201804, China. E-mail: lisa@tongji.edu.cn

^b Institute of New Energy for Vehicles, Tongji University, Shanghai 201804, China

^c Department of Nuclear Science and Engineering and Department of Materials Science and Engineering, Massachusetts Institute of Technology, Cambridge, MA 02139, USA. E-mail: liju@mit.edu

† Electronic supplementary information (ESI) available. See DOI: 10.1039/c9cc02006c

Inspired by the recent understanding of reversible oxygen anion-redox reaction in cathode materials, it behooves one to activate the anion-redox contributions and pursue hybrid cation- and anion-redox (HAC) capacities in cathode materials to boost the energy density.^{5–7} While the reversible $O^{2-} \leftrightarrow O^-$ (oxo \leftrightarrow peroxo) transition has been demonstrated in Li-rich $Li_{1+x}M_{1-x}O_2$ with a layered structure, such as $yLi_2MnO_3 \cdot (1-y)LiMO_2$ ($M = Mn, Ni, Co$ mixture), there have been very few attempts in spinel $Li_4Mn_5O_{12}$, also written as $Li(Mn_{5/3}Li_{1/3})O_4$, where 1/6 of the Mn ions in the classical $LiMn_2O_4$ spinel structure are replaced by Li ions.^{4,12} Generally speaking, there is a mixture of ionic and covalent bonding between the cations (Li, Mn) and oxygen. While Li–O bonding is strongly ionic, Mn_{3d}/O_{2p} have a significant orbital overlap and thus Mn–O has a stronger covalent bonding character, which stabilizes O^{2-} and pushes $U^{eq}(O^{1-/2-})$ to higher voltages. However, the degree of ionic bonding increases with 1/6 of the Mn ions being replaced by Li ions, and as a result, $U^{eq}(O^{1-/2-})$ can move to lower voltages, at around 4 V vs. Li^+/Li . Thus, the oxygen ions can, in principle, deliver extra m, a -capacities before the voltage gets so high (like > 5 V) that the Al current collector corrodes or the electrolyte decomposes too violently.¹³

Herein, we report a simple and scalable solid-state method to synthesize nanoscale $Li_4Mn_5O_{12}$ -like particulates at a low temperature. After an activation process, both the cation-redox capacity at ~ 3 V vs. Li^+/Li originating from $Mn^{3.5+} \rightarrow Mn^{4+}$ and the anion-redox capacity at ~ 4 V vs. Li^+/Li provided by $O^{2-} \rightarrow O^-$ are obtained. The reaction proceeds theoretically as



with a theoretical capacity of $243.9 \text{ mA h g}^{-1}$, where the anion-redox capacity contributes 44% ($m = 2, a = 1/6, 108.4 \text{ mA h g}^{-1}$) and the cation-redox capacity contributes 56% ($p = 2.5, c = 0.5, 135.5 \text{ mA h g}^{-1}$), and the reaction coordinate of eqn (1) is kinked as illustrated in Fig. 1a. In practice, a high discharge specific capacity of 212 mA h g^{-1} and energy density of 668 Wh kg^{-1} were achieved in half cells.

The low-temperature solid-state synthesis process is illustrated in Fig. S1 (ESI[†]). The $Li_4Mn_5O_{12}$ -like cathode was prepared through a solid-state process, which is very simple and scalable. The as-obtained sample was then characterized by X-ray diffraction (XRD), and the XRD pattern (Fig. 1b) could be approximately indexed to the $Li_4Mn_5O_{12}$ phase (JCPDS no. 46-0810). Based on the Rietveld refinement, the lattice parameters of a monoclinic unit cell are $a = 8.128 \text{ \AA}$ and unit cell volume = 537.130 \AA^3 , closely approaching the values reported by Takada, which confirms its $Li_4Mn_5O_{12}$ -like motif.¹⁴ From the Scherrer equation and Williamson–Hall analysis,¹⁵ we found that the particle size was 9.57 nm and the microstrain fluctuation (slope of broadening vs. $4 \sin \theta$) was ~ -0.00246 (as shown in Fig. 1c). The small, but negative, value of -0.00246 is unusual and means that the particle sizes are so small that the anisotropic surface stress and other factors give a non-uniform strain distribution. The sub-10 nm nanoparticulate nature (due to the low- T synthesis, which prevented coarsening) is believed to play a key role in the ability to utilize the anion-redox capacity. When Mn stays at 4+ (the red leg of the reaction coordinate in

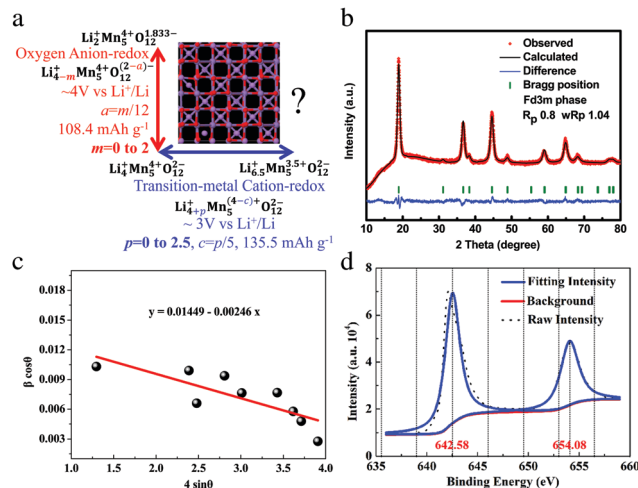


Fig. 1 (a) Hybrid oxygen anion-redox and transition-metal cation-redox reaction coordinates of reaction (1): $Li_2^+Mn_5^{4+}O_{12}^{1.833-} \leftrightarrow Li_{4-m}^+Mn_5^{3.5+}O_{12}^{2-a-} \leftrightarrow Li_{6.5}^+Mn_5^{3.5+}O_{12}^{2-}$. The inset shows the spinel $Li(Mn_{5/3}Li_{1/3})O_4$ with a long-range order of 1/6 Li_{Mn} substitutions. However, we believe our material may have significant disordering, or a random solid solution, of these 1/6 Li_{Mn} substitutions, due to the low-temperature synthesis, (b) Rietveld refinement XRD patterns, (c) Williamson–Hall plots with linear fitting, (d) Mn 2p XPS spectra.

Fig. 1a), the electronic conductivity has to be low due to the lack of transition-metal polaron conduction (unlike the blue leg, where there is an abundant mixture of Mn^{4+} and Mn^{3+}). Therefore, one relies more on the surface conduction and electron tunneling mechanisms, which favors smaller particles. On the other hand, while the smaller particles have favorable kinetics, they also have more side reactions with the electrolyte, so an optimal particle size should exist.

X-ray photoelectron spectroscopy (XPS) was carried out (Fig. 1d) to identify the valence state of Mn. The fitting peaks are at 642.58 eV and 654.08 eV, which are the characteristic peaks of $Mn^{4+} 2p_{3/2}$ and $Mn^{4+} 2p_{1/2}$, respectively.^{16,17} The microstructure and morphology of the $Li_4Mn_5O_{12}$ -like powders were also observed through field emission scanning electron microscopy (FE-SEM), as shown in Fig. S2a and S2b (ESI[†]). Secondary microparticles with a diameter of around $5 \mu\text{m}$ can be seen (Fig. S2a, ESI[†]), and a closer observation in Fig. S2b (ESI[†]) reveals that the secondary particles are self-assembled by the primary nanoparticles. Such a hierarchical microstructure could also be identified by transmission electron microscopy (TEM) (Fig. S3, ESI[†]), where subunits of $\sim 20\text{--}100 \text{ nm}$ agglomerated and formed $\sim 5 \mu\text{m}$ particles. It is generally believed that such nano-sized crystallinity could effectively accommodate the strain of Jahn–Teller distortion through the slippage at the domain wall boundaries, and thus is beneficial to the stability of the cathode material.^{18–20}

The $Li_4Mn_5O_{12}$ -like cathode was then electrochemically examined in coin cells. After an initial charging process $Li_4^+Mn_5^+O_{12}^{2-} \rightarrow Li_{4-m}^+Mn_5^{4+}O_{12}^{(2-a)-}$ (that was largely abandoned in conventional samples due to lack of reversibility), the $Li_4Mn_5O_{12}$ -like cathode seems to be activated and delivers a capacity of 210 mA h g^{-1} (at 0.1C) in the first discharge, when the net-additional lithium was provided by the counter electrode. In the following 20 cycles, the specific capacity increases gradually and reaches a maximum value

of 212 mA h g⁻¹ (a discharge energy density of 668 W h kg⁻¹) at the 20th cycle. This would be impossible without the anion-redox *m,a*-contributions. As discussed before, since the tetravalent manganese ions cannot be oxidized, the first charge capacity of 82.6 mA h g⁻¹ that we measured must arise from the O-redox reaction, which turns out to be highly reversible in the following cycles. The progress coordinate of reaction (1) contains a directional change as illustrated in Fig. 1a at Li₄Mn₅O₁₂²⁻, with one part given by the red anion-redox and the other part given by the blue cation-redox leg. From the voltage profile, there is a plateau at 2.8 V vs. Li⁺/Li that corresponds to lithium insertion into the octahedral sites of the spinel Li₄Mn₅O₁₂ accompanied by the reduction of manganese ions Li₄Mn₅O₁₂²⁻ ↔ Li_{4+p}Mn₅^{(4-c)+}O₁₂²⁻. It is commonly believed that Jahn–Teller distortion has no chance of causing a phase change/structural collapse as long as the oxidation state of the manganese ions stays above 3.5.⁴

Our Li₄Mn₅O₁₂-like cathode, which was prepared by a simple one-pot synthesis and was not optimized, could still maintain a capacity of 153 mA h g⁻¹ and an energy density of 470 W h kg⁻¹ at room temperature after 145 cycles, as shown in Fig. 2c. Interestingly, the capacity exhibits an increasing trend during the initial 20 cycles, which we believe is associated with an activation process. From the 30th cycle, the capacity starts to decay, possibly originating from the dissolution of manganese with a disproportionation reaction of Mn³⁺(solid) → Mn⁴⁺(solid) + Mn²⁺(solution) and the onset of Jahn–Teller distortion at the end of discharge.⁴ The discharge potential of the Li₄Mn₅O₁₂-like cathode is stable (at 3.1 V) during cycling, almost without any drop (in Fig. 2b).

The full cells were assembled by pairing the Li₄Mn₅O₁₂-like cathode against a Li_xSn anode³² and tested at a current density of 100 mA g⁻¹ between 1.0 and 4.1 V at room temperature. As shown in Fig. S6a and S6b (ESI[†]), the initial discharge capacity reaches 213 mA h g⁻¹. After 45 cycles, the capacity stabilizes at 204 mA h g⁻¹ with hardly any capacity attenuation.

Based on the analysis above, the discharge capacities of the Li₄Mn₅O₁₂-like cathode include hybrid cation- and anion-redox capacities. Here, we separate the capacities into two parts in a discharge curve of the 20th cycle, which are attributed to the cation-redox and anion-redox processes, as shown in Fig. 3a and b. The cation-redox process (Mn³⁺/Mn⁴⁺) covers the area at about 3 V vs. Li⁺/Li. The capacity due to this process is 108.4 mA h g⁻¹, corresponding to a reaction of Li₄Mn₅O₁₂²⁻ + 2Li⁺ + 2e⁻ ↔ Li₆Mn₅O₁₂^{3.6+}. The capacity attributed by the anion-redox process is 103.6 mA h g⁻¹, which can be described as a reaction of Li₄Mn₅O₁₂²⁻ - 1.9Li⁺ - 1.9e⁻ ↔ Li_{2.1}Mn₅O₁₂^{1.84-}. To clarify the underlying mechanism of the anion-redox contribution, we conducted a Differential Electrochemical Mass Spectrometry (DEMS) test under a galvanostatic condition, as shown in Fig. 3c. During the first charging process, O₂ was generated once the potential exceeded 3.4 V, implying that there was O²⁻ oxidation. From the second cycle, no O₂ generation was detected, indicative of a possible existence of solid-state peroxide, which was further confirmed through XPS characterization (Fig. 3d). From the O 1s spectrum, there is an obvious difference in the oxidation state of the oxygen atoms in the Li₄Mn₅O₁₂-like cathode at different SOCs.

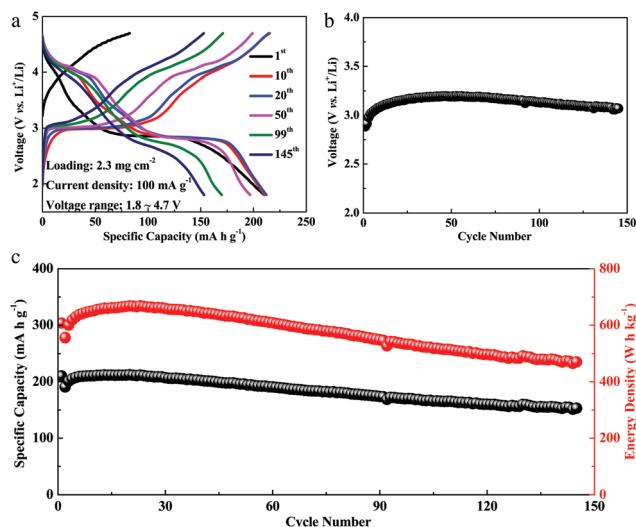


Fig. 2 (a) Charge/discharge curves of the Li₄Mn₅O₁₂-like half cells from the 1st cycle to the 145th cycle at a current density of 100 mA g⁻¹ among 1.8–4.7 V versus Li⁺/Li at room temperature, (b) evolution of average discharge voltage during cycling, (c) cycling performance of Li₄Mn₅O₁₂-like half cells.

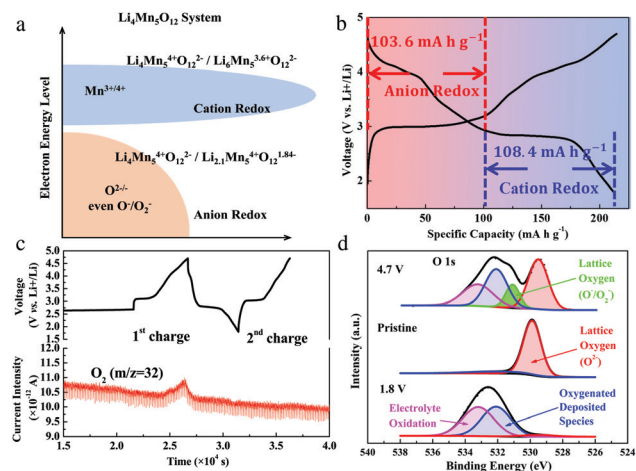


Fig. 3 (a) Schematic illustration of cation- and anion-redox processes in the Li₄Mn₅O₁₂ system, (b) the distinguished cation- and anion-redox capacities in a discharge curve of the 20th cycle respectively, (c) DEMS analysis of the Li₄Mn₅O₁₂-like cathode in a half cell tested with a constant current density of 100 mA g⁻¹ and a voltage window of 1.8–4.7 V versus Li⁺/Li, (d) XPS spectra of a pristine Li₄Mn₅O₁₂-like sample, a sample charged to 4.7 V and a sample discharged to 1.8 V.

Specifically, for a pristine sample, a peak at 529.5 eV that corresponds to the O²⁻ anions of the crystalline network^{21,22} and a peak at 532.1 eV that might be associated with a weakly absorbed surface species, such as CO₂, were observed. At 4.7 V, two new peaks occur. The peak at 531.1 eV is related to the onset of a new component with a lower electronic density of oxide ions than O²⁻ ions, indicating that O²⁻ ions were oxidized to O⁻/O²⁻ or under-coordinated oxygen atoms.²¹ It disappeared when the sample was discharged to 1.8 V. We anticipate that the reversible appearance/disappearance of the 531.1 eV peak during the charge/discharge process reveals the reversibility of

the anion-redox reaction. In addition, the other peak at 533.2 eV corresponds to electrolyte oxidation.^{22,23}

We are intrigued as to why our samples manifest a reversible capacity $\text{Li}_4^+\text{Mn}_5^{4+}\text{O}_{12}^{2-} \rightarrow \text{Li}_2^+\text{Mn}_5^{4+}\text{O}_{12}^{1.833-}$ for hundreds of charge/discharge cycles. In addition to the sub-10 nm primary particle size (9.57 nm), we speculate that the partial destruction of chemical ordering could also play a role. Recall that $\text{Li}_4\text{Mn}_5\text{O}_{12}$ is better understood as $\text{Li}(\text{Mn}_{5/3}\text{Li}_{1/3})\text{O}_4$, where 1/6 of the Mn sites in the classical LiMn_2O_4 spinel structure are replaced by Li ions.^{4,12} However, the $\text{Li}_4\text{Mn}_5\text{O}_{12}$ illustrated in Fig. 1a is a perfect compound with chemical ordering, meaning those 1/6 Li_{Mn} substitutions are perfectly long-range ordered and not an alloy. However, due to the 400 °C low-*T* synthesis (most solid-state synthesis takes place at >600 °C),²⁴ the ordering of these Li_{Mn} substitutions in our samples may not be perfect, and may form a random solid solution, despite the large agreement in the XRD peaks in Fig. 1b with the reference crystal. That is, while the expression “Li-rich spinel $\text{Li}(\text{Mn}_{5/3}\text{Li}_{1/3})\text{O}_4$ ” should be correct as a chemical formula, those Li_{Mn} substitutions may have more randomized positions. We may also have Mn occupying some of the original tetrahedral Li sites of the classical LiMn_2O_4 spinel, or other kinds of local ionic disorders. For reference, the $\text{Mn}_{\text{tetrahedral/octahedral}}^{4+}$ has a Shannon–Prewitt crystal radius of 0.53 Å/0.67 Å, while $\text{Li}_{\text{tetrahedral/octahedral}}^+$ has a Shannon–Prewitt crystal radius of 0.73 Å/0.90 Å.²⁵ This kind of random solid-solution behavior may explain the sloping voltage curve in the first charge in Fig. S6a (ESI†).^{26–28} Since the detailed Li–O–Mn and Li–O–Li geometries greatly affect the equilibrium oxygen redox potential,^{29,30} as well as the internal charge-transfer rates (e.g., $\text{O}^{1-} \rightarrow \text{O}^{2-}$ and $\text{Mn}^{3+} \rightarrow \text{Mn}^{4+}$ together), we speculate that this kind of occupancy disorder and random-solution behavior with the redox-activated dynamic rearrangements of ions⁶ could facilitate an oxygen redox reaction, also assisted, of course, by the small particle size and electron tunneling.

In summary, a cobalt-free $\text{Li}_4\text{Mn}_5\text{O}_{12}$ -like nanoparticulate cathode, synthesized at a low temperature of 400 °C (most solid-state synthesis of cathode materials occurs at above 600 °C^{24,31}), demonstrates a high reversible capacity of 212 mA h g⁻¹ with hybrid cation- and anion-redox contributions. Compared to commercial LiFePO_4 , LiCoO_2 , and $\text{Li}(\text{Ni}_x\text{Co}_y\text{Mn}_{1-x-y})\text{O}_2$, it not only has a lower cost, but also higher capacities (Fig. S9, ESI†). Furthermore, the cycling stability is also acceptable. The $\text{Li}_4\text{Mn}_5\text{O}_{12}$ -like cathode maintains a capacity of 153 mA h g⁻¹ after 145 cycles at a current density of 100 mA g⁻¹. The electrochemical performance of the full cell with this $\text{Li}_4\text{Mn}_5\text{O}_{12}$ -like cathode and lithium tin alloy anode is impressive with a high capacity of 214 mA h g⁻¹ and almost without any capacity fading after 45 cycles. Results above show that this Li-rich spinel, also known as $\text{Li}(\text{Mn}_{5/3}\text{Li}_{1/3})\text{O}_4$, is attractive for further investigations as a lithium-ion battery cathode.

Conflicts of interest

There are no conflicts to declare.

References

- 1 A. R. Armstrong and P. G. Bruce, *Nature*, 1996, **381**, 499.
- 2 M. M. Thackeray, A. de Kock, M. H. Rossouw, D. Liles, R. Bittihn and D. Hoge, *J. Electrochem. Soc.*, 1992, **139**, 363–366.
- 3 E. Ferg, R. Gummow, A. De Kock and M. Thackeray, *J. Electrochem. Soc.*, 1994, **141**, L147–L150.
- 4 M. M. Thackeray, *Prog. Solid State Chem.*, 1997, **25**, 1–71.
- 5 Z. Zhu, A. Kushima, Z. Yin, L. Qi, K. Amine, J. Lu and J. Li, *Nat. Energy*, 2016, **1**, 16111.
- 6 W. E. Gent, K. Lim, Y. Liang, Q. Li, T. Barnes, S.-J. Ahn, K. H. Stone, M. McIntire, J. Hong and J. H. Song, *Nat. Commun.*, 2017, **8**, 2091.
- 7 X. Rong, E. Hu, Y. Lu, F. Meng, C. Zhao, X. Wang, Q. Zhang, X. Yu, L. Gu and Y.-S. Hu, *Joule*, 2018, **3**, 503–517.
- 8 T. Takada, H. Hayakawa, E. Akiba, F. Izumi and B. C. Chakoumakos, *J. Power Sources*, 1997, **68**, 613–617.
- 9 Y. Jiang, J. Xie, G. Cao and X. Zhao, *Electrochim. Acta*, 2010, **56**, 412–417.
- 10 Y. Fu, H. Jiang, Y. Hu, L. Zhang and C. Li, *J. Power Sources*, 2014, **261**, 306–310.
- 11 Z. Xie, H. Eikhuemelo, J. Zhao, C. Cain, W. Xu and Y. Wang, *J. Electrochem. Soc.*, 2015, **162**, A1523–A1529.
- 12 M.-J. Lee, E. Lho, P. Bai, S. Chae, J. Li and J. Cho, *Nano Lett.*, 2017, **17**, 3744–3751.
- 13 L. Suo, W. Xue, M. Gobet, S. G. Greenbaum, C. Wang, Y. Chen, W. Yang, Y. Li and J. Li, *Proc. Natl. Acad. Sci. U. S. A.*, 2018, 201712895.
- 14 T. Takada, H. Hayakawa and E. Akiba, *J. Solid State Chem.*, 1995, **115**, 420–426.
- 15 A. K. Zak, W. A. Majid, M. E. Abrishami and R. Yousefi, *Solid State Sci.*, 2011, **13**, 251–256.
- 16 V. Di Castro, G. Polzonetti, G. Contini, C. Cozza and B. Paponetti, *Surf. Interface Anal.*, 1990, **16**, 571–574.
- 17 B. J. Tan, K. J. Klabunde and P. M. A. Sherwood, *J. Am. Chem. Soc.*, 1991, **113**, 855–861.
- 18 H. Wang, Y. I. Jang and Y. M. Chiang, *Electrochem. Solid-State Lett.*, 1999, **2**, 490–493.
- 19 Y. I. Jang, B. Huang, Y. M. Chiang and D. R. Sadoway, *Electrochem. Solid-State Lett.*, 1998, **1**, 13–16.
- 20 Y. Shao-Horn, S. A. Hackney, A. R. Armstrong, P. G. Bruce, R. Gitzendanner, C. S. Johnson and M. M. Thackeray, *J. Electrochem. Soc.*, 1999, **146**, 2404–2412.
- 21 J.-C. Dupin, D. Gonbeau, P. Vinatier and A. J. P. C. C. P. Levasseur, *Phys. Chem. Chem. Phys.*, 2000, **2**, 1319–1324.
- 22 M. Sathiya, G. Rousse, K. Ramesha, C. Laisa, H. Vezin, M. T. Sougrati, M.-L. Doublet, D. Foix, D. Gonbeau and W. J. N. m. Walker, *Nat. Mater.*, 2013, **12**, 827.
- 23 R. Dedryvere, D. Foix, S. Franger, S. Patoux, L. Daniel and D. Gonbeau, *J. Phys. Chem. C*, 2010, **114**, 10999–11008.
- 24 L. Li, Y. Xu, X. Sun, R. Chang, Y. Zhang, X. Zhang and J. Li, *Adv. Energy Mater.*, 2018, **8**, 1801064.
- 25 R. D. Shannon, *Acta Crystallogr., Sect. A: Cryst. Phys., Diffr., Theor. Gen. Crystallogr.*, 1976, **32**, 751–767.
- 26 J. Niu, A. Kushima, X. Qian, L. Qi, K. Xiang, Y.-M. Chiang and J. Li, *Nano Lett.*, 2014, **14**, 4005–4010.
- 27 H. Liu, F. C. Strobridge, O. J. Borkiewicz, K. M. Wiaderek, K. W. Chapman, P. J. Chupas and C. P. Grey, *Science*, 2014, **344**, 1252817.
- 28 M. Z. Bazant, *Acc. Chem. Res.*, 2013, **46**, 1144–1160.
- 29 J. Lee, A. Urban, X. Li, D. Su, G. Hautier and G. Ceder, *Science*, 2014, **343**, 519–522.
- 30 A. Urban, I. Matts, A. Abdellahi and G. Ceder, *Adv. Energy Mater.*, 2016, **6**, 1600488.
- 31 J. L. Shi, D. D. Xiao, M. Ge, X. Yu, Y. Chu, X. Huang, X. D. Zhang, Y. X. Yin, X. Q. Yang and Y. G. Guo, *Adv. Mater.*, 2018, **30**, 1705575.
- 32 H. Xu, S. Li, C. Zhang, X. L. Chen, W. J. Liu, Y. H. Zheng, Y. Xie, Y. H. Huang and J. Li, *Energy Environ. Sci.*, 2019, DOI: 10.1039/C9EE01404G.

Supplementary Information

Method

Synthesis of $\text{Li}_4\text{Mn}_5\text{O}_{12}$ -like. We used a low-temperature solid-state synthesis method to prepare spinel $\text{Li}_4\text{Mn}_5\text{O}_{12}$ -like samples. First, MnCO_3 (Aladdin, 99.95%) was mixed with $\text{LiOH}\cdot\text{H}_2\text{O}$ (Adamas, 99%). The molar ratio of MnCO_3 : $\text{LiOH}\cdot\text{H}_2\text{O}$ was 5:4. After ground for 1 h, the obtained mixture was sintered at 400°C for 12 h under air atmosphere to get the final material.

Material characterizations. X-ray diffraction was performed on Rigaku Ultima IV. It was operated in the 2θ value range of 10° to 80° with a $2^\circ/\text{min}$ scanning rate. The morphology of the $\text{Li}_4\text{Mn}_5\text{O}_{12}$ -like sample was identified by Quanta 200 field emission scanning electron microscope (FESEM). The HRTEM images were taken on a transmission electron microscope JEM-2100F with accelerating voltage of 200 kV. X-ray photoelectron spectroscopy (XPS) measurement was carried out by use of ESCALAB 250Xi.

Electrochemical tests. CR2025-type coin cells, assembled in a glove box filled with dry argon gas, were used for electrochemical tests. A coin cell consisted of a positive electrode, an anode, ceramic membrane and organic electrolyte. To fabricate the positive electrode, active materials and carbon black (electron conduction) were ground with the weight ratio of 90:5. Then the as-prepared materials were mixed with polyvinylidene fluoride (PVDF) binder (95:5, weight ratio) in appropriate amount of N-methylpyrrolidone (NMP), using magnetic stirring to mix fully. The obtained slurry

was cast onto an aluminum foil current collector. Then, it was dried at 80°C overnight in vacuum. The organic electrolyte was 1mol/L LiPF₆ in a mixture of equal volumes of ethylene carbonate (EC) and dimethyl carbonate (DMC). For half cells and full cells, the anodes were lithium metal and lithium-tin alloy respectively. The electrochemical tests were carried out on a battery test system (Neware). Electrochemical impedance spectroscopy (EIS) data was performed on a CHI600A Electrochemical workstation (Chinster, Shanghai, China), with 5mV ac excitation over a frequency range of 1 mHz to 100 kHz. Cyclic voltammogram (CV) test was performed at a scan rate of 0.1 mV s⁻¹ among voltage range of 1.8 V to 4.7 V (vs. Li⁺/Li) by a CHI600A Electrochemical workstation (Chinster, Shanghai, China).

Result and discussion

The low-temperature solid-state synthesis process is illustrated in Fig. S1. Li₄Mn₅O₁₂-like cathode is prepared through a solid-state process, which is very simple and scalable.

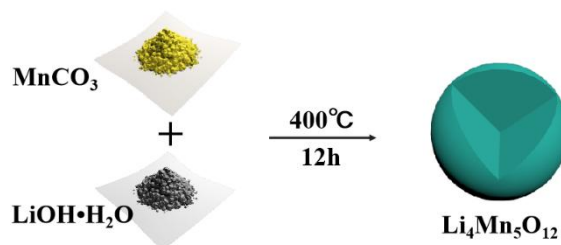


Fig. S1. The synthesis schematic diagram of Li₄Mn₅O₁₂-like nanoparticulates.

The microstructure and morphology of Li₄Mn₅O₁₂-like powders are also observed through field emission scanning electron microscopy (FE-SEM), as shown in Fig. S2a and S2b. Secondary microparticles with a diameter of around 5 μm could be seen (Fig. S2a) and closer observation in Fig. S2b reveals that the secondary particles are self-assembled by primary nanoparticles.

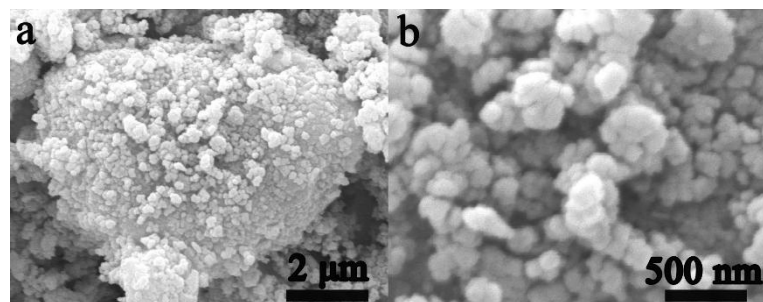


Fig. S2. (a) and (b) SEM images of $\text{Li}_4\text{Mn}_5\text{O}_{12}$ -like nanoparticulates, which self-assemble into secondary particles.

From the high-resolution transmission electron microscopy (HRTEM) image in Fig. S3, interplanar spacing of 0.471 nm and 0.239 nm, which are corresponded to the [111] and [222] planes of spinel $\text{Li}_4\text{Mn}_5\text{O}_{12}$ structure, respectively, are identified. It is generally believed that such nano-sized crystallinity could effectively accommodate the strain of Jahn-Teller through slippage at the domain wall boundaries, and thus is beneficial to the stability of cathode material.¹⁻³

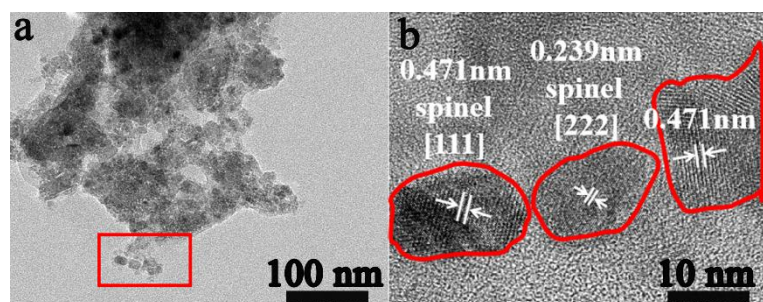


Fig. S3. (a)TEM and (b)HRTEM images of $\text{Li}_4\text{Mn}_5\text{O}_{12}$ -like nanoparticulates, which self-assemble into secondary particles.

The CV curve (in Fig. S4) also indicates that there are two lithium storage processes, corresponding to two redox peaks at ~ 2.8 V and ~ 4 V respectively during discharge process of $\text{Li}_4\text{Mn}_5\text{O}_{12}$ -like cathode.

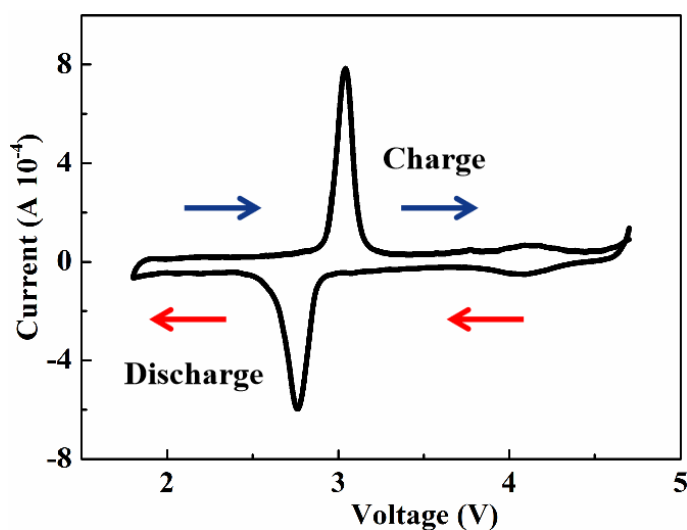


Fig. S4. CV curve of $\text{Li}_4\text{Mn}_5\text{O}_{12}$ -like.

Thanks to the cubic structure of spinel $\text{Li}_4\text{Mn}_5\text{O}_{12}$ with three-dimensional Li diffusion channels, this cathode shows good rate performance with small impedance during cycling, as revealed in Fig. S5.

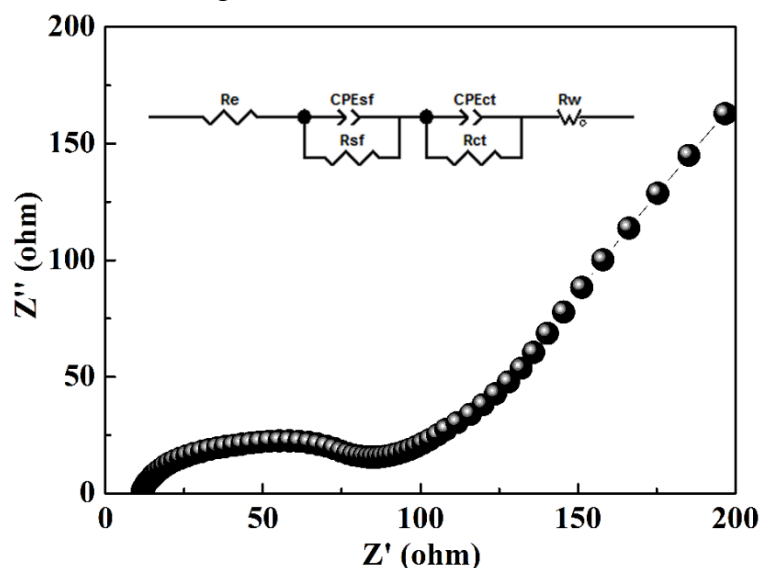


Fig. S5. Equivalent circuit model and Nyquist plots of $\text{Li}_4\text{Mn}_5\text{O}_{12}$ -like.

The full cells were assembled by pairing the $\text{Li}_4\text{Mn}_5\text{O}_{12}$ -like cathode against Li_xSn anode⁴ and tested at a current density of 100 mA g^{-1} between 1.0 and 4.1 V at room temperature. As shown in Fig. S6a and S6b, the initial discharge capacity reaches 213 mA h g^{-1} . After 45 cycles, the capacity stabilizes at 204 mA h g^{-1} with hardly any capacity attenuation.

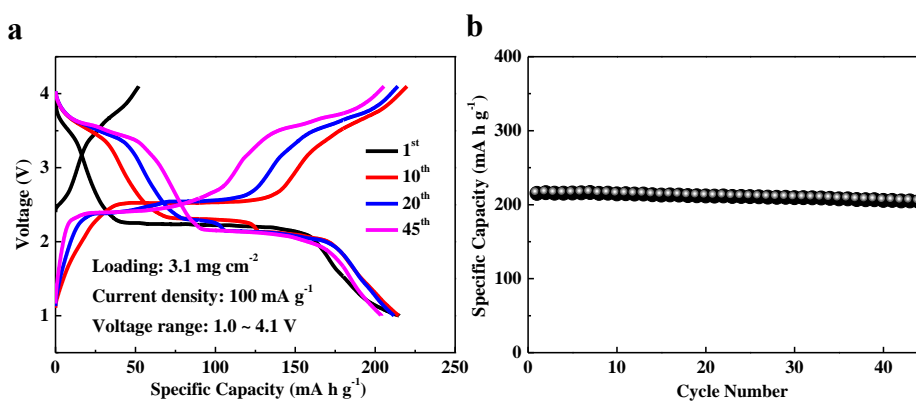


Fig. S6. (a) Charge/discharge curves of $\text{Li}_4\text{Mn}_5\text{O}_{12}$ -like full cells from the 1st cycle to the 45th cycle at a current density of 100 mA g^{-1} among 1.0 ~ 4.1 V at room temperature, (b) cycling performance of $\text{Li}_4\text{Mn}_5\text{O}_{12}$ -like full cells.

In Fig. S7, cation- and anion-redox capacities evolving over cycles were examined individually, where an anion-redox capacity increment during the first 30 cycles was observed, probably due to an activation process of oxygen. In the subsequent cycles, a slow decline that might be related to oxygen release could be found. Meanwhile, cation-redox capacity deteriorates gradually with prolonged cycling, which is possibly

attributed to the dissolution of manganese and the damage of structure.

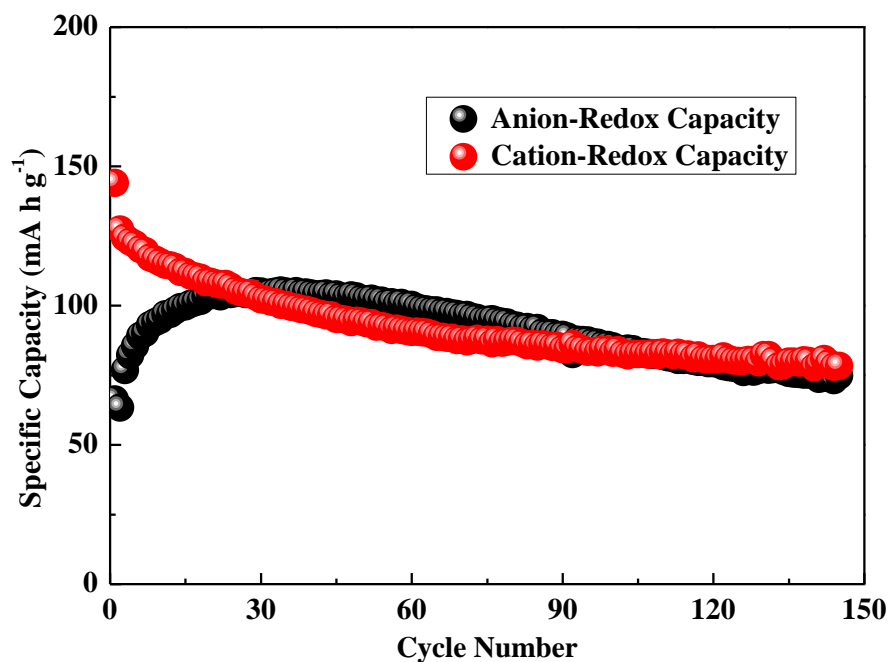


Fig. S7. The cation- and anion-redox capacities evolving over cycles of $\text{Li}_4\text{Mn}_5\text{O}_{12}$ -like cathode.

In Fig. S8, the derivative capacity vs. voltage of $\text{Li}_4\text{Mn}_5\text{O}_{12}$ -like cathode is calculated by the data of the 20th cycle (presented in Fig. 3b). The main redox peaks are at ~ 2.8 V and ~ 4 V, which correspond to two reactions above mentioned.

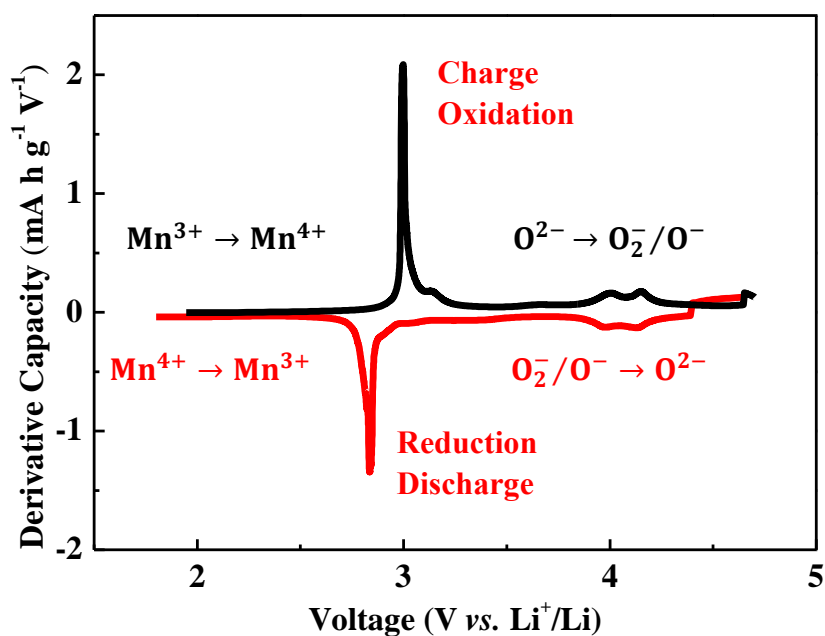


Fig. S8. Derivative capacity vs. voltage curve of $\text{Li}_4\text{Mn}_5\text{O}_{12}$ system during the 20th cycle. $\text{Li}_4\text{Mn}_5\text{O}_{12}$ -like cathode could have excellent cost-performance ratio. Compared

with the benchmark cathode materials, such as LiFePO_4 , LiCoO_2 , LiNiO_2 and $\text{Li}(\text{Ni}_x\text{Co}_y\text{Mn}_{1-x-y})\text{O}_2$, our $\text{Li}_4\text{Mn}_5\text{O}_{12}$ -like cathode can deliver a high capacity of 213 mA h g^{-1} , which behaves better than LiFePO_4 (162 mA h g^{-1}), LiCoO_2 (140 mA h g^{-1}), and $\text{LiNi}_{1/3}\text{Co}_{1/3}\text{Mn}_{1/3}\text{O}_2$ (200 mA h g^{-1}).⁵⁻⁷ The cost of our cathode material is less than $\$ 5.72 \text{ kg}^{-1}$, which is one fifth of the cost of LiCoO_2 ($\$ 26.24 \text{ kg}^{-1}$), a quarter of the cost of $\text{LiNi}_{1/3}\text{Co}_{1/3}\text{Mn}_{1/3}\text{O}_2$ ($\$ 20.99 \text{ kg}^{-1}$) and about one third of the cost of LiFePO_4 ($\$ 12.72 \text{ kg}^{-1}$), as exhibited in Fig. S9.

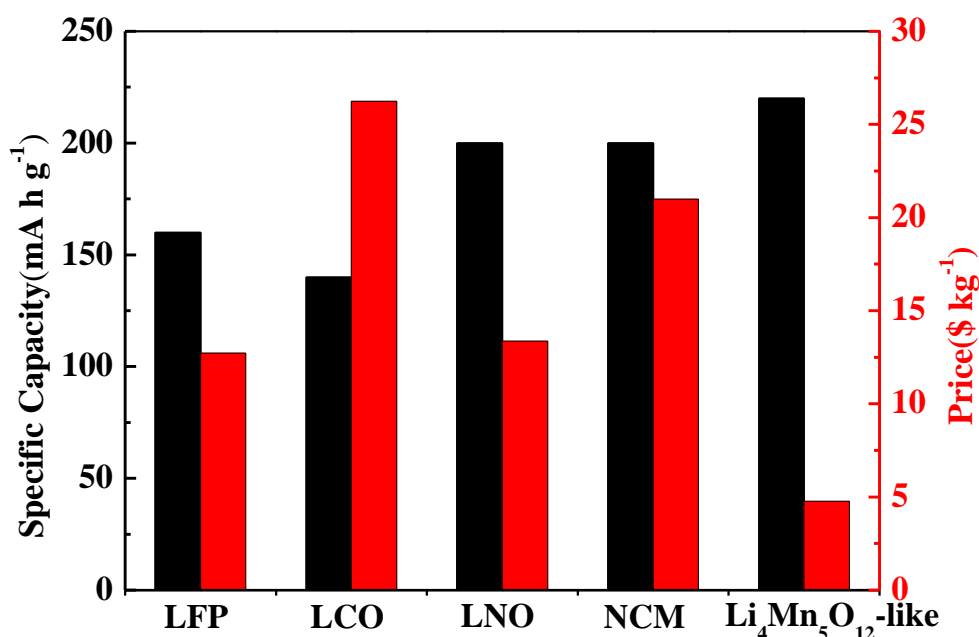


Fig. S9. Specific capacities and price of LiFePO_4 (LFP), LiCoO_2 (LCO), LiNiO_2 (LNO), $\text{Li}(\text{Ni}_x\text{Co}_y\text{Mn}_{1-x-y})\text{O}_2$ (NCM) and $\text{Li}_4\text{Mn}_5\text{O}_{12}$ -like.

The tap density of well-prepared $\text{Li}_4\text{Mn}_5\text{O}_{12}$ -like cathode is about 3 g cm^{-3} . Therefore, the volumetric energy density of $\text{Li}_4\text{Mn}_5\text{O}_{12}$ -like cathode is estimated to be as high as 2060 W h L^{-1} . This value is quite competitive, compared to LFP and even NCM, but we believe it could be further optimized because, at the present stage, the primary particles is very small. And the volumetric energy density remains at 1450 W h L^{-1} after 145 cycles.

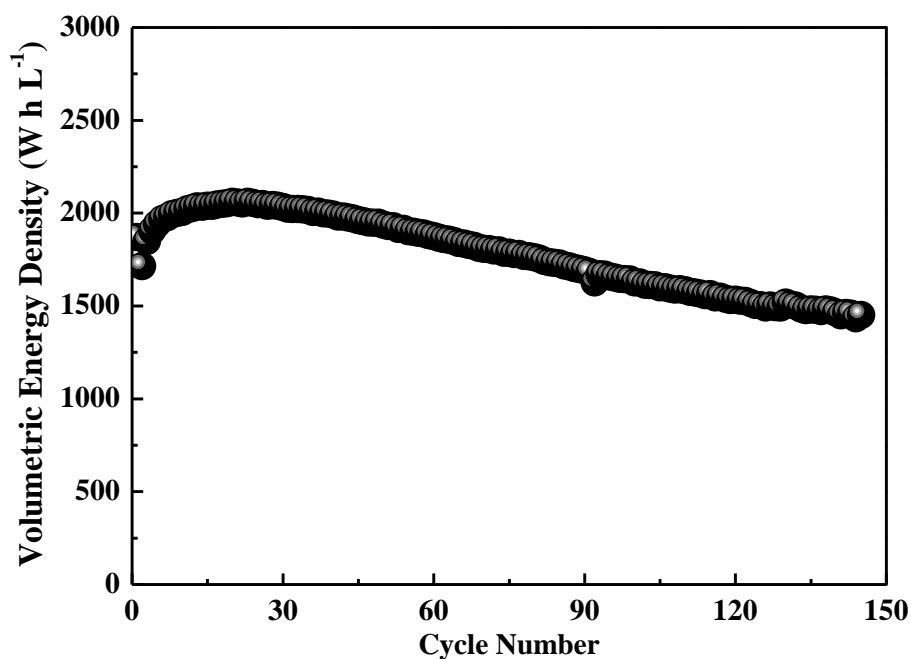


Fig. S10. Volumetric energy density of $\text{Li}_4\text{Mn}_5\text{O}_{12}$ -like half cells from the 1st cycle to the 145th cycle at a current density of 100 mA g^{-1} within a voltage window of $1.8 \sim 4.7 \text{ V}$ versus Li^+/Li at room temperature.

Table S1 Linear fitting data of Williamson-Hall (W-H) plots (in Fig. 1c).

Equation	$y = a + b \cdot x$		
Weight	No Weighting		
Residual Sum of Squares	1.68255E-5		
Pearson's r	-0.81481		
Adj. R-Square	0.6159		
		Value	Standard Error
B	Intercept	0.01449	0.00203
B	Slope	-0.00246	6.62668E-4

References

1. H. Wang, Y. I. Jang and Y. M. Chiang, *Electrochemical and Solid-State Letters*, 1999, **2**, 490-493.
2. Y. I. Jang, B. Huang, Y. M. Chiang and D. R. Sadoway, *Electrochemical and Solid-State Letters*, 1998, **1**, 13-16.

3. Y. Shao - Horn, S. A. Hackney, A. R. Armstrong, P. G. Bruce, R. Gitzendanner, C. S. Johnson and M. M. Thackeray, *Journal of the Electrochemical Society*, 1999, **146**, 2404-2412.
4. H. Xu, S. Li, C. Zhang, X. L. Chen, W. J. Liu, Y. H. Zheng, Y. Xie, Y. H. Huang and J. Li, *Energy Environ. Sci.*, 2019, 10.1039/C9EE01404G.
5. A. Yamada, S.-C. Chung and K. Hinokuma, *Journal of the Electrochemical Society*, 2001, **148**, A224-A229.
6. T. Ohzuku, A. Ueda, M. Nagayama, Y. Iwakoshi and H. Komori, *Electrochimica Acta*, 1993, **38**, 1159-1167.
7. N. Yabuuchi and T. Ohzuku, *Journal of Power Sources*, 2003, **119**, 171-174.